Song et al. *NPG Asia Materials* (2023) 15:43
https://doi.org/10.1038/s41427-023-00489-6

NPG Asia Materials

ARTICLE Open Access

Realizing metallicity in Sr_2IrO_4 thin films by high-pressure oxygen annealing

Zhen Song[1,2], You-Shan Zhang[3], Jing-Yi Shen[4,2], Bing Lin[1,2], Jie Wu[2], Ping-Hua Xiang[3], Chun-Gang Duan[3] and Rui-Hua He[2]

Abstract

Perovskite iridates are a promising material platform for hosting unconventional superconductivity. Transport measurements of Sr_2IrO_4 thin-film field-effect transistors are expected to provide irrefutable evidence for the existence of superconductivity. However, these experiments have revealed a remarkably robust insulating state over wide electron and hole doping ranges; this finding is in contrast to the case of the bulk material, in which metallicity appears upon moderate electron doping by substituting cations in place of Sr. The nature of this robust insulating state and whether any metallic state can be realized in the Sr_2IrO_4 thin film are two remaining challenges that preclude further progress in the search for superconductivity in this system. Here, we show that this insulating state is enhanced in Sr_2IrO_4 thin films by thermal annealing under vacuum conditions, while it can be destroyed upon annealing in an oxygen atmosphere within restricted ranges of oxygen pressure, annealing temperature and ion substitution levels. The resulting films exhibit metallic transport behavior near room temperature and a metal–insulator crossover at ~200 K. Our results point to the potentially important roles of the oxygen vacancies at different atomic sites in the formation of the robust insulating state and the new metallic state and to their interplay in the Sr_2IrO_4 thin film. This finding opens new possibilities in the search for unconventional superconductivity by further tailoring the as-found metallic state in properly oxygen-annealed Sr_2IrO_4 thin films.

Introduction

Unconventional superconductivity remains a central topic of condensed matter physics[1–3]. Special attention has been given to compounds with crystal and electronic structures similar to those of cuprates with the hope of finding new superconductors and understanding the origin of cuprate superconductivity[4–9]. In addition to the few related systems that have been primarily focused on[4,9], the 5*d* transition-metal oxide system Sr_2IrO_4 has attracted considerable interest. Undoped Sr_2IrO_4 features a unique Mott insulating state as a result of the interplay between strong spin–orbit coupling and Coulomb interactions[10–13]. Melting of this spin–orbit Mott phase upon electron and hole doping has been theoretically predicted to yield unconventional superconductivity[14,15]. Consistent with this finding, angle-resolved photoemission[16] and scanning tunneling microscopy[17] experiments have shown spectroscopic signatures consistent with a *d*-wave superconducting gap in surface electron-doped Sr_2IrO_4 at low temperatures. Nevertheless, transport evidence for the zero-resistance state is required to establish the occurrence of superconductivity in doped Sr_2IrO_4.

Electron[18–20] and hole[21,22] doping through cation substitution in bulk Sr_2IrO_4 can weaken and destroy the undoped insulating state at relatively high temperatures (>100 K) without the superconductivity observed at relatively low temperatures. Restricted by the solubility limits for various substitutional dopants, bulk doping cannot reach the sufficiently high electron or hole doping levels predicted for superconductivity to emerge. The ionic liquid gating technique presents a general solution to this problem, and it is capable of realizing ambipolar doping in

Correspondence: Rui-Hua He (heruihua@westlake.edu.cn)
[1]Department of Physics, Fudan University, 200433 Shanghai, China
[2]Research Center for Industries of the Future & Key Laboratory for Quantum Materials of Zhejiang Province, Department of Physics, Westlake University, 310024 Hangzhou, Zhejiang, China
Full list of author information is available at the end of the article

excess of 10% in quite a few material systems[23–27]. However, in the case of Sr_2IrO_4, liquid gating experiments on thin-film samples have revealed remarkably robust insulating behaviors over enormously wide electron and hole doping ranges[28,29]. The origin of this behavior is unknown to date, but it may occur due to factors introduced by the gating technique[27,30,31] and/or factors intrinsic to the thin-film samples[20,32]. Indications for the latter reasoning come from the observed increases in resistivity upon (Ce) electron[33] and (charge-transfer) hole[34] doping of the Sr_2IrO_4 thin films, in contrast to the bulk cases[18–20,22]. To our knowledge, no metallic state has thus far been found in the Sr_2IrO_4 thin film regardless of the thin film growth and doping methods[28,29,33–35]. The nature of the robust insulating state and whether any metallic state can be realized in the Sr_2IrO_4 thin film are two remaining questions[36]. Their resolutions are prerequisites for making progress on the important issue of unconventional superconductivity in Sr_2IrO_4.

In this work, we perform a systematic study of the effects of thermal annealing both under vacuum conditions and in an oxygen atmosphere on the transport property of the Sr_2IrO_4 thin film. We find that the robust insulating state is enhanced by vacuum annealing and weakened by oxygen annealing. This state can be destroyed near room temperature after oxygen annealing at ~50 atm and ~570 °C in a pristine thin film, where a new metallic state appears. These observations outline an emerging transport phase diagram of the Sr_2IrO_4 thin film featuring an interplay between the robust insulating state and the new metallic state. We argue that while the robust insulating state is likely dominated by the defect scattering effect of planar oxygen vacancies, the new metallic state likely reflects an intrinsic bulk-like property of the IrO_2 planes with effective electron doping due to apical oxygen vacancies. This finding provides a new perspective for a unified understanding of the puzzling transport properties of the Sr_2IrO_4 thin film and suggests a new pathway for discovering superconductivity in Sr_2IrO_4 around the as-found metallic state.

Materials and methods

High-quality thin films of pristine Sr_2IrO_4 and 5% Ce-doped Sr_2IrO_4 [$(Sr_{0.95}Ce_{0.05})_2IrO_4$] were grown on atomically flat $(LaAlO_3)_{0.3}(Sr_2AlTaO_6)_{0.35}$ (LSAT) (001) substrates by the pulsed laser deposition (PLD) method using a KrF excimer laser (wavelength of 248 nm) as in our previous study[33]. Ceramic targets of stoichiometric Sr_2IrO_4 and $(Sr_{0.95}Ce_{0.05})_2IrO_4$ were fabricated by conventional solid-state reactions. The energy density of the pulsed laser was approximately 0.3 J cm^{-2}, and the frequency was 5 Hz. During thin-film deposition, the substrate temperature was maintained at 800 °C with an oxygen partial pressure of 0.13 Pa. Upon the completion of the deposition, the sample was first cooled to 650 °C in an oxygen atmosphere of 0.13 Pa and then cooled to room temperature at a 5×10^4 Pa oxygen pressure and a cooling rate of 20 °C min^{-1}. All films were ~20 nm thick, and the growth rate was ~0.02 nm s^{-1}. Thermal annealing of the as-grown films was conducted in a chamber under vacuum conditions exceeding 1×10^{-10} mbar. Thermal annealing of the as-grown films in an oxygen atmosphere was conducted in a high-pressure tube furnace (OTF-1200X-HP-55, MTI Co.) with high-purity oxygen gas (purity > 99.995%). The oxygen pressure was initially set and subsequently maintained for each annealing at a given pressure value, with the aid of an electromagnetic valve for automatic gas release (deviation < ±2%), during temperature increase (rate of 10 °C min^{-1}) and maintenance (duration of 1 h) stages. During the cooling stage (rate of −10 °C min^{-1}), the oxygen pressure naturally decreased with decreasing temperature for a fixed amount of oxygen gas inside the furnace. The structural properties of the films before and after oxygen annealing (Fig. S1) were characterized by four-circle X-ray diffraction (Bruker D8 Discover) with a Cu $K_{\alpha1}$ wavelength of 1.5406 Å. The chemical states of the films were characterized by X-ray photoelectron spectroscopy (XPS; Thermo Scientific ESCALAB Xi+) with Al Kα radiation (1486.6 eV).

The electrical transport properties of the samples were measured with the four-point probe method to effectively eliminate the lead and contact resistance from the measurement. Gold electrodes with thicknesses of 50 nm were deposited on the surface of each sample by thermal evaporation to ensure good electrical contact. A Keithley 6221 current source and a Keithley 2182A nanovoltmeter were used for the resistance measurement along the crystallographic *a*-axis or *b*-axis of the thin film. The geometric dimensions of each sample were accurately measured with an optical microscope, and the *a*-axis (or *b*-axis) resistivities of the samples were calculated based on the measured resistance values and cross-sectional areas of the thin films. Transport measurements were conducted in a cryostat over the temperature range of 3.5–300 K at a cooling/heating rate of 1 K min^{-1}. To minimize the effects of possible sample-to-sample variation due to the growth process, each study of the annealing temperature (T_A) or pressure of oxygen atmosphere (P_{OA}) dependence was performed on samples in small pieces (~2.5 mm × 5 mm) that were cut from the same large piece (10 mm × 10 mm) of the as-grown sample using a wire saw.

Results

The temperature dependence of the electrical resistivity (R–T curve) of the as-grown Sr_2IrO_4 thin film is shown in Fig. 1a. The resistivity of the sample decreases with

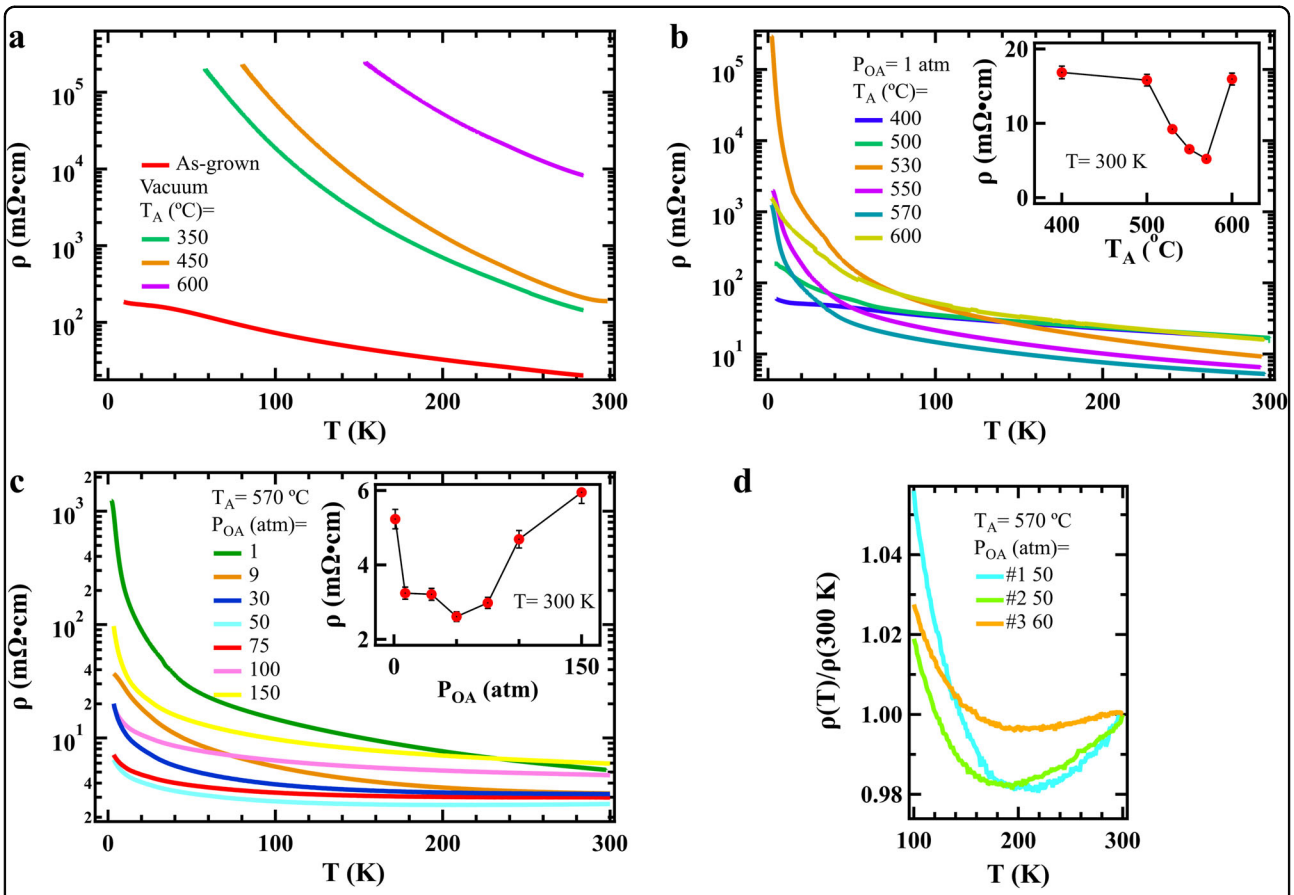

Fig. 1 Temperature dependence of the electrical resistivity (*R–T* curves) of the Sr_2IrO_4 thin films subject to different annealing treatments. **a** Vacuum annealing at different T_A as indicated. **b** Oxygen annealing under $P_{OA} = 1$ atm at different T_A values as indicated. **c** Oxygen annealing at $T_A = 570$ °C under different P_{OA} values as indicated. The insets in **b** and **c** summarize the resistivity values at room temperature of the corresponding *R–T* curves as a function of T_A and P_{OA}, respectively. **d** *R–T* curves (resistivity normalized at room temperature) of samples annealed under nearly optimal conditions ($P_{OA} \sim 50$ atm, $T_A = 570$ °C). Error bars in the insets of **b** and **c** mainly reflect the reproducibility of the resistivity measurement on the given sample and the sample-to-sample variations in multiple samples (if available) grown/annealed/measured under nominally the same conditions.

increasing temperature, which depicts typical insulating behavior. Figure 1a shows the *R–T* curves of Sr_2IrO_4 thin films after thermal annealing at different temperatures ($T_A = 350$, 450, and 600 °C) under vacuum conditions. The resistivity of the $T_A = 350$ °C film at room temperature is nearly one order of magnitude higher than that of the as-grown film. Upon a further increase in T_A, the sample resistivity increases, and the insulating behavior persists.

Figure 1b presents the *R–T* curves of Sr_2IrO_4 thin films after thermal annealing at different temperatures ($T_A = 400$–600 °C) in a 1 atm oxygen atmosphere. As T_A increases toward 570 °C, the resistivity of the oxygen-annealed film at room temperature decreases gradually and reaches a minimum value of 5.24 mΩ cm for $T_A = 570$ °C, which is close to a quarter of the value of the as-grown sample. A further increase in T_A leads to a rapid increase in resistivity. This phenomenon points to an overall nonmonotonic T_A-dependent evolution of the resistivity across $T_A = 570$ °C, which is exemplified in the inset of Fig. 1b for the resistivity value at room temperature.

Figure 1c shows the *R–T* curves of Sr_2IrO_4 thin films after thermal annealing at $T_A = 570$ °C in an oxygen atmosphere at various high pressures ($P_{OA} = 1$–150 atm). With increasing P_{OA}, the sample resistivity at room temperature first decreases rapidly for $P_{OA} < 9$ atm and slows before increasing under high P_{OA} values (inset of Fig. 1c). The room-temperature resistivity reaches a minimum value of 2.61 mΩ cm at $P_{OA} = 50$ atm, which is approximately 8 times smaller than the value for the as-grown sample. Interestingly, nonmonotonic *R–T* curves can be robustly found in the samples annealed in oxygen under similar conditions at $T_A = 570$ °C and $P_{OA} \sim 50$ atm, which commonly highlights a metal–insulator crossover at ~200 K, as shown in Fig. 1d.

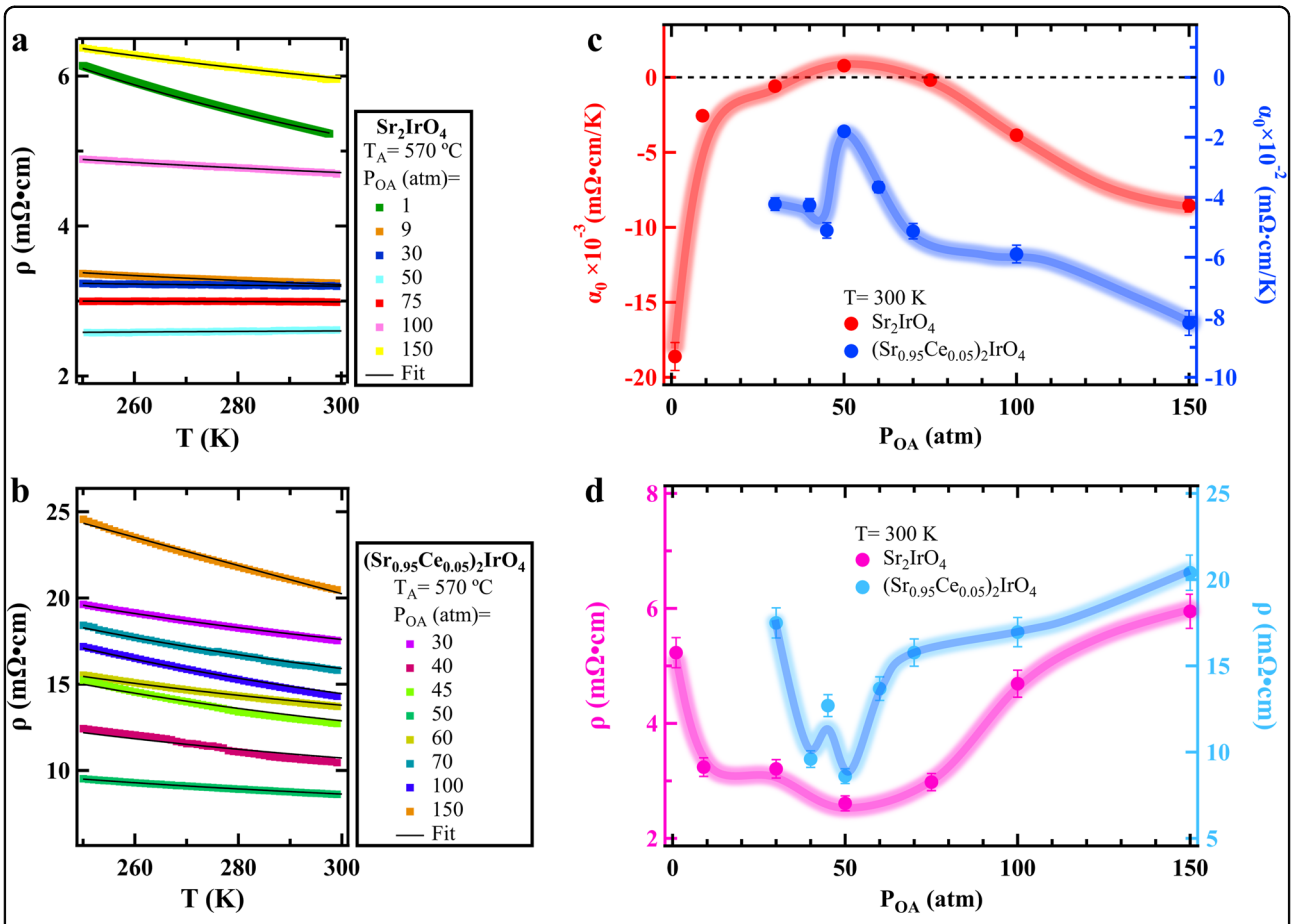

Fig. 2 Temperature- and P_{OA}-dependent evolution characteristics of the electrical resistivities for the Sr_2IrO_4 and $(Sr_{0.95}Ce_{0.05})_2IrO_4$ thin films after oxygen annealing at $T_A = 570$ °C. a, **b** *R–T* curves of the Sr_2IrO_4 (**a**) and $(Sr_{0.95}Ce_{0.05})_2IrO_4$ (**b**) thin films annealed under different P_{OA} values, with each fitted by $\rho(T) = \rho_0[1 + \alpha_0(T - T_0)]$ in the temperature range between 250 and 300 K. **c** Fitted coefficient α_0 and **d** room-temperature resistivity extracted from **a** and **b** for both types of samples under different P_{OA} values. Color ribbons in **c** and **d** are guides to the eye based on the spline interpolations to the experimental data. Error bars in the insets of **c** and **d** mainly reflect the reproducibility of the resistivity measurement on the given sample and the sample-to-sample variations in multiple samples (if available) grown/annealed/measured under nominally the same conditions.

The temperature dependence of the resistivity of a semiconductor can be generally described by the formula $\rho(T) = \rho_0[1 + \alpha_0(T - T_0)]$, where ρ_0, α_0 and T_0 are material-specific parameters[37]. Here, we apply this formula to fit the same *R–T* curves as shown in Fig. 1c and reproduced in Fig. 2a in the vicinity of room temperature (250–300 K), and we obtain the coefficient α_0. Figure 2c depicts the evolution of α_0 with increasing P_{OA}. With increasing P_{OA}, the magnitude of α_0 first decreases and then increases. α_0 is generally negative, which is indicative of the insulating behavior of the sample. The value becomes positive in the vicinity of $P_{OA} = 50$ atm, which is consistent with the metallic behavior observed near room temperature in Fig. 1d.

As a comparison, we perform transport measurements on the $(Sr_{0.95}Ce_{0.05})_2IrO_4$ thin films. The resistivity of the as-grown $(Sr_{0.95}Ce_{0.05})_2IrO_4$ thin film is a few times larger than that of the pristine film (cf. Figs. S2 and 1a), which is consistent with our earlier report[33]. Oxygen annealing at $T_A = 570$ °C at an increasing P_{OA} leads to an initial decrease in the resistivity of the Ce-doped film near room temperature followed by an increase for $P_{OA} > 50$ atm, which is reminiscent of the case of the pristine sample (Fig. 2d). The optimal P_{OA} value for obtaining the minimum resistivity is close to 50 atm in both cases, regardless of the difference in Ce doping. However, important differences are noted. The resistivity of the $(Sr_{0.95}Ce_{0.05})_2IrO_4$ thin films is overall higher than that of the pristine films. The metal–insulator crossover observed at $\sim P_{OA} = 50$ atm in the pristine samples is absent in the Ce-doped samples (Fig. S2).

The results of the coefficients α_0 are similarly defined for the R–T curves near room temperature of $(Sr_{0.95}Ce_{0.05})_2IrO_4$ thin films, and they are shown in Fig.

2c. With increasing P_{OA}, the magnitude of α_0 exhibits nonmonotonic behavior and reaches its minimum value at 50 atm, which is similar to the pristine case. However, α_0 is always negative, and no significant change is observed at $\sim P_{OA} = 50$ atm, as in the pristine case, which is consistent with the absence of a metallic state in the Ce-doped films. The above results suggest that the robust insulating state is enhanced while the metallic state is weakened by Ce doping in the Sr_2IrO_4 thin film.

Discussion

Our results obtained from the study of thermal annealing under vacuum conditions and in an oxygen atmosphere on the pristine and Ce-doped Sr_2IrO_4 thin films are consistent with an emerging transport phase diagram of the Sr_2IrO_4 thin film, as schematically depicted in Fig. 3. A hypothetical resistivity (ρ) surface near room temperature is shown as a function of the Ce doping (x) and oxygen content (p). The pink/blue (dashed) curve on the $x = 0/x = 0.05$ plane is the hypothetical $\rho - p$ curve for the pristine/Ce-doped sample near room temperature. Specifically, the pink curve can be divided into three regimes, as labeled in Fig. 3.

The as-grown state of the Sr_2IrO_4 thin film sits close to the boundary between Regimes I and II, where oxygen vacancies created during the thin film growth are likely abundant in both the apical and planar oxygen sites. Consistent with this finding, our XPS measurement on the as-grown Sr_2IrO_4 thin film suggests the coexistence of 4+ and 3+ chemical states of Ir (Fig. S3). The planar oxygen vacancies (on the IrO_2 planes) can serve as defect scattering centers that effectively disrupt the in-plane electrical conduction, which is a well-known effect for the case of CuO_2 planes in cuprates[38–40]. Depending on the density of oxygen vacancies, the resulting state can have insulating transport behavior dominated by planar oxygen vacancies rather than carrier concentration. This state is expected to be minimally affected by the electrostatic doping of carriers; it can be further enhanced by thermal annealing under vacuum conditions, increasing the number of planar oxygen vacancies (with decreasing oxygen content moving the system toward/further into Regime I in Fig. 3). This trend offers a simple explanation for the robust insulating state of the Sr_2IrO_4 thin film.

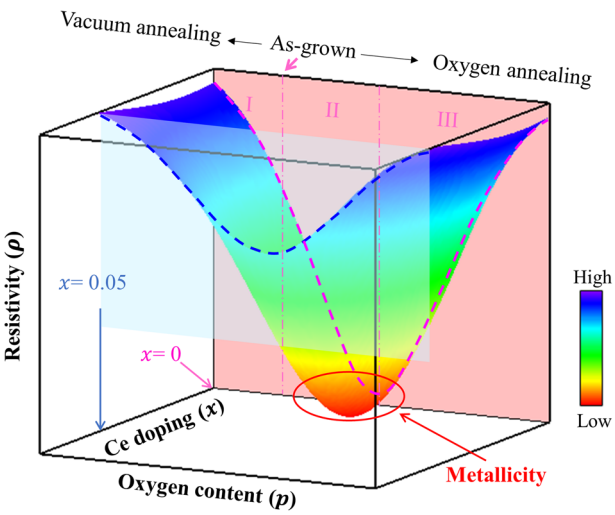

Fig. 3 Schematic summary of the effects of Ce doping and oxygen content on the electrical resistivity near room temperature for the Sr_2IrO_4 thin films. See text for related descriptions.

Thermal annealing in the oxygen atmosphere upon increasing T_A and/or P_{OA} causes the oxygen vacancies to be increasingly filled (with increasing oxygen content moving the system toward/further into Regime II in Fig. 3). Consistent with this finding, our X-ray diffraction measurements on the oxygen annealed thin films show notable c-axis contractions that have been commonly observed in oxide materials upon filling oxygen vacancies[41–43] (Fig. S1). Thus, we still do not know which types of oxygen vacancies are filled. In this regard, we note that the planar Ir–O bond length is smaller than the apical bond length in Sr_2IrO_4[20,44]. On thermodynamic grounds, a larger bonding strength of the planar Ir–O bond suggests that an oxygen atom can bind more easily with the planar oxygen vacancy than with the apical oxygen vacancy, as their binding reduces the energy of the system by the amount of Ir–O bond strength. A caveat is that the thermodynamic energy minimum associated with the filling-in of a planar oxygen vacancy can be preceded by some energy barrier that tends to block the access of the oxygen atom to the planar oxygen vacancy. We speculate that this sort of energy barrier might have been overcome due to the increased mobility of oxygen atoms during the high-pressure oxygen annealing of our samples at high temperatures. This phenomenon can potentially lead to the planar oxygen vacancies being preferentially filled in over the apical oxygen vacancies.

As a result, the robust insulating state is weakened, and the inherent in-plane conduction can eventually be restored, as all planar oxygen sites are replenished. Moreover, the IrO_2 planes remain electron-doped due to the unfilled apical oxygen vacancies that act as effective donors. Metallic transport can thus occur, as in the case of bulk electron-doped Sr_2IrO_4. This finding can explain why a metallic state can be found in the pristine samples under proper oxygen annealing conditions.

Oxygen annealing with further increasing T_A and/or P_{OA} causes the apical oxygen vacancies to be filled in (with increasing oxygen content that moves the system toward/further into Regime III in Fig. 3). The metallic transport is gradually weakened due to the decrease in electron doping until the intrinsic (insulating) transport of

the undoped bulk-like Sr_2IrO_4 eventually recovers. This phenomenon can explain why this metallic state only exists within a restricted parameter space of thermal annealing (circled region in Fig. 3).

Hereafter (somewhere in Regime III), the intrinsic hole-doped property may become apparent upon further oxygen annealing that can create interstitial oxygen atoms as acceptors. While the insulating transport at half-filling is expected to be weakened by hole doping, the rate of weakening appears lower than the case of electron doping according to bulk doping studies[18,19,21,22].

Concerning the effect of 5% Ce doping, we note that it is sufficient to cause a major reduction in the resistivity and induce metallicity in bulk Sr_2IrO_4[20]. In thin films, we have previously found that increasing Ce substitution leads to *c*-axis contraction and weakening of the magnetic order[33], which is similar to the known effects of increasing Ce substitution in the bulk[20]. This finding implies that Ce is an effective electron donor in the Sr_2IrO_4 thin films. Consistent with this trend, our XPS measurement on the as-grown $(Sr_{0.95}Ce_{0.05})_2IrO_4$ thin film shows a higher Ir^{3+} content than the pristine sample (Fig. S3). Surprisingly, our resistivity measurements show that 5% Ce doping strengthens the robust insulating state and weakens the new metallic state. The latter aspect, in particular, cannot be easily understood if the substituted Ce ions only serve as effective donors[20] that can promote in-plane conduction. Instead, both aspects can be rationalized if Ce doping introduces additional defect scattering sites[33] in the IrO_2 planes that cannot be removed by oxygen annealing.

The above heuristic picture highlights the potentially central role played by the oxygen vacancies at different atomic sites in shaping the transport phase diagram of the Sr_2IrO_4 thin film due to the interplay between the robust insulating state and the new metallic state found in this study. This finding suggests that while the robust insulating state is likely dominated by the defect scattering effect of planar oxygen vacancies, the new metallic state likely reflects an intrinsic bulk-like property of the IrO_2 planes with effective electron doping due to apical oxygen vacancies. This phenomenon provides a new perspective for a unified understanding of the puzzling transport properties of the Sr_2IrO_4 thin film. While this perspective should be scrutinized further in experiments with oxygen annealing, it suggests a new pathway for finding superconductivity in iridates by modifying this metallic state in the Sr_2IrO_4 thin film. Regarding directions for modification, our study suggests that Ce doping might not be sufficiently effective for Sr_2IrO_4 thin films. La doping is reported to reduce the thin film resistivity[28,35], unlike Ce doping[33]. This finding seems to indicate that the defect scattering effect may not be as strong in the case of La doping, which is beneficial for the appearance of metallicity in oxygen-annealed Sr_2IrO_4 thin films. In any case, using properly oxygen-annealed thin films as substrates for ionic liquid gating experiments has a favorable outcome.

Conclusion

The effects of thermal annealing in a vacuum and oxygen atmosphere on the transport property of the Sr_2IrO_4 thin film are investigated. We show that the robust insulating state found in earlier experiments is enhanced by vacuum annealing and weakened by oxygen annealing. This state can even be destroyed after oxygen annealing under ~50 atm at ~570 °C in the pristine thin film, where a new metallic state appears near room temperature. A unified picture is proposed to understand these new transport findings on the Sr_2IrO_4 thin film, which highlights the potentially central role played by the oxygen vacancies at different atomic sites in the formation of the robust insulating state and the new metallic state and by their interplay. We establish the properly oxygen-annealed Sr_2IrO_4 thin film as a viable platform for finding superconductivity in iridates.

Note added after submission: It has been drawn to our attention that two earlier studies reported resistivity measurements based on electrochemical oxygen doping of Sr_2IrO_4 in different forms[45] and vacuum annealing of polycrystalline Sr_2IrO_4[46], which is qualitatively consistent with the results reported in this work.

Acknowledgements

The work at Westlake University was supported by the National Key R&D Program of China (Grant No. 2022YFA1402200), National Natural Science Foundation of China (Grants Nos. 12274353, 11874053, 12174318), Zhejiang Provincial Natural Science Foundation of China (LZ19A040001), Foundation of Westlake Multidisciplinary Research Initiative Center (MRIC20210101), and Westlake Instrumentation and Service Center for Physical Sciences. The work at East China Normal University (ECNU) was supported by the National Natural Science Foundation of China (Grant No. 11874149).

Author details

[1]Department of Physics, Fudan University, 200433 Shanghai, China. [2]Research Center for Industries of the Future & Key Laboratory for Quantum Materials of Zhejiang Province, Department of Physics, Westlake University, 310024 Hangzhou, Zhejiang, China. [3]Key Laboratory of Polar Materials and Devices (Ministry of Education), Department of Electronics, East China Normal University, 200241 Shanghai, China. [4]Department of Physics, Zhejiang University, 310027 Hangzhou, Zhejiang, China

Author contributions

R.-H.H. conceived the project, secured funding, and guided the investigations. Y.-S.Z. grew the sample under the guidance of P.-H.X. and C.-G.D. Z.S. conducted the annealing experiments with help from J.-Y.S. and B.L. and analyzed the data. Z.S. and R.-H.H. wrote the manuscript with input from J.W. and P.-H.X. All authors contributed to the discussions.

Competing interests

The authors declare no competing interests.

Supplementary information The online version contains supplementary material available at https://doi.org/10.1038/s41427-023-00489-6.

Received: 10 March 2023 Revised: 6 June 2023 Accepted: 20 June 2023.
Published online: 4 August 2023

References

1. Lee, P. A., Nagaosa, N. & Wen, X. G. Doping a Mott insulator: physics of high temperature superconductivity. *Rev. Mod. Phys.* **78**, 17–85 (2004).
2. Stewart, G. R. Superconductivity in iron compounds. *Rev. Mod. Phys.* **83**, 1589–1652 (2011).
3. Keimer, B., Kivelson, S. A., Norman, M. R., Uchida, S. & Zaanen, J. From quantum matter to high-temperature superconductivity in copper oxides. *Nature* **518**, 179–186 (2015).
4. Maeno, Y. & Hashimoto, H. Superconductivity in a layered perovskite without copper. *Nature* **372**, 532–534 (1994).
5. Anisimov, V. I., Bukhvalov, D. & Rice, T. M. Electronic structure of possible nickelate analogs to the cuprates. *Phys. Rev. B* **59**, 7901–7906 (1999).
6. Lee, K. W. & Pickett, W. E. Infinite-layer $LaNiO_2$: Ni^{1+} is not Cu^{2+}. *Phys. Rev. B* **70**, 165109 (2004).
7. Chaloupka, J. & Khaliullin, G. Orbital order and possible superconductivity in $LaNiO_3/LaMO_3$ superlattices. *Phys. Rev. Lett.* **100**, 016404 (2008).
8. Hansmann, P. et al. Turning a nickelate Fermi surface into a cupratelike one through heterostructuring. *Phys. Rev. Lett.* **103**, 016401 (2009).
9. Li, D. et al. Superconductivity in an infinite-layer nickelate. *Nature* **572**, 624–627 (2019).
10. Kim, B. J. et al. Novel $J_{\mathrm{eff}} = 1/2$ Mott state induced by relativistic spin–orbit coupling in Sr_2IrO_4. *Phys. Rev. Lett.* **101**, 076402 (2008).
11. Kim, B. J. et al. Phase-sensitive observation of a spin-orbital Mott state in Sr_2IrO_4. *Science* **323**, 1329–1332 (2009).
12. Moon, S. J. et al. Dimensionality-controlled insulator–metal transition and correlated metallic state in 5*d* transition metal oxides $Sr_{n+1}Ir_nO_{3n+1}$ ($n = 1$, 2, and ∞). *Phys. Rev. Lett.* **101**, 226402 (2008).
13. Cao, G. & Schlottmann, P. The challenge of spin–orbit-tuned ground states in iridates: a key issues review. *Rep. Prog. Phys.* **81**, 042502 (2018).
14. Wang, F. & Senthil, T. Twisted Hubbard model for Sr_2IrO_4: magnetism and possible high temperature superconductivity. *Phys. Rev. Lett.* **106**, 136402 (2011).
15. Meng, Z. Y., Kim, Y. B. & Kee, H. Y. Odd-parity triplet superconductivity in multi-orbital materials with strong spin-orbit coupling: applications to doped Sr_2IrO_4. *Phys. Rev. Lett.* **113**, 177003 (2014).
16. Kim, Y. K., Sung, N. H., Denlinger, J. D. & Kim, B. J. Observation of a *d*-wave gap in electron-doped Sr_2IrO_4. *Nat. Phys.* **12**, 37–41 (2015).
17. Yan, Y. J., Ren, M. Q., Xu, H. C., Xie, B. P. & Feng, D. L. Electron-doped Sr_2IrO_4: an analogue of hole-doped cuprate superconductors demonstrated by scanning tunneling microscopy. *Phys. Rev. X* **5**, 041018 (2015).
18. Ge, M. et al. Lattice-driven magnetoresistivity and metal-insulator transition in single-layered iridates. *Phys. Rev. B* **84**, 100402 (2011).
19. Chen, X. et al. Influence of electron doping on the ground state of $(Sr_{1-x}La_x)_2IrO_4$. *Phys. Rev. B* **92**, 075125 (2015).
20. Huang, H., Ji, P., Xie, Y., Han, H. & Ge, B. Exploration of the bond angle and charge carrier density by rare-earth doping in Sr_2IrO_4. *Phys. Rev. Mater.* **4**, 115001 (2020).
21. Qi, T. F. et al. Spin-orbit tuned metal-insulator transitions in single-crystal $Sr_2Ir_{1-x}Rh_xO_4 (0 \le x \le 1)$. *Phys. Rev. B* **86**, 125105 (2012).
22. Chikara, S. et al. Charge partitioning and anomalous hole doping in Rh-doped Sr_2IrO_4. *Phys. Rev. B* **95**, 060407 (2017).
23. Ueno, K. et al. Electric-field-induced superconductivity in an insulator. *Nat. Mater.* **7**, 855–858 (2008).
24. Scherwitzl, R. et al. Electric-field control of the metal–insulator transition in ultrathin $NdNiO_3$ films. *Adv. Mater.* **22**, 5517–5520 (2010).
25. Ye, J. T. et al. Liquid-gated interface superconductivity on an atomically flat film. *Nat. Mater.* **9**, 125–128 (2010).
26. Nakano, M. et al. Collective bulk carrier delocalization driven by electrostatic surface charge accumulation. *Nature* **487**, 459–462 (2012).
27. Leighton, C. Electrolyte-based ionic control of functional oxides. *Nat. Mater.* **18**, 13–18 (2019).
28. Ravichandran, J. et al. Ambipolar transport and magneto-resistance crossover in a Mott insulator, Sr_2IrO_4. *J. Phys.: Condens. Matter* **28**, 505304 (2016).
29. Lu, C. et al. Dual gate control of bulk transport and magnetism in the spin–orbit insulator Sr_2IrO_4. *Phys. Rev. B* **91**, 104401 (2015).
30. Jeong, J. et al. Suppression of metal–insulator transition in VO_2 by electric field-induced oxygen vacancy formation. *Science* **339**, 1402–1405 (2013).
31. Li, M. et al. Suppression of ionic liquid gate-induced metallization of $SrTiO_3(001)$ by oxygen. *Nano Lett.* **13**, 4675–4678 (2013).
32. Souri, M. et al. Crossover between Mott and Efros–Shklovskii variable-range hopping in Sr_2IrO_4 epitaxial thin films by misfit strain and isovalent doping. *J. Appl. Phys.* **126**, 185101 (2019).
33. Zhang, Y. et al. Effect of Ce doping on the structural, transport and magnetic properties of Sr_2IrO_4 epitaxial films. *J. Phys. D: Appl. Phys.* **54**, 405304 (2021).
34. Wen, F. et al. Interface-engineered hole doping in $Sr_2IrO_4/LaNiO_3$ heterostructure. *N. J. Phys.* **21**, 103009 (2019).
35. Li, M. Y. et al. Tuning the electronic structure of Sr_2IrO_4 thin films by bulk electronic doping using molecular beam epitaxy. *Chin. Phys. Lett.* **32**, 057402 (2015).
36. Lu, C. & Liu, J. M. The $J_{\mathrm{eff}} = 1/2$ antiferromagnet Sr_2IrO_4: a golden avenue toward new physics and functions. *Adv. Mater.* **32**, 1904508 (2020).
37. Alenitsyn, A. G., Butikov, E. I. & Kondratyev, A. S. *Concise Handbook of Mathematics and Physics* 331–332 (CRC Press, Boca Raton, 1997).
38. Matsunaka, D., Rodulfo, E. T. & Kasai, H. Effects of oxygen-vacancies in high-temperature cuprate superconductors. *Solid State Commun.* **134**, 355–360 (2005).
39. Hiroi, Z., Kobayashi, N. & Takano, M. Probable hole-doped superconductivity without apical oxygens in $(Ca, Na)_2CuO_2Cl_2$. *Nature* **371**, 139 (1994).
40. Naito, M., Krockenberger, Y., Ikeda, A. & Yamamoto, H. Reassessment of the electronic state, magnetism, and superconductivity in high-T_c cuprates with the Nd_2CuO_4 structure. *Physica C* **523**, 28–54 (2016).
41. Adler, S. B. Chemical expansivity of electrochemical ceramics. *J. Am. Ceram. Soc.* **84**, 2117–2119 (2001).
42. Aschauer, U., Pfenninger, R., Selbach, S. M., Grande, T. & Spaldin, N. A. Strain-controlled oxygen vacancy formation and ordering in $CaMnO_3$. *Phys. Rev. B* **88**, 054111 (2013).
43. Ullmann, H. & Trofimenko, N. Estimation of effective ionic radii in highly defective perovskite type oxides from experimental data. *J. Alloy. Compd.* **316**, 153–158 (2001).
44. Bhatti, I. N., Rawat, R., Banerjee, A. & Pramanik, A. K. Temperature evolution of magnetic and transport behavior in 5*d* Mott insulator Sr_2IrO_4: significance of magneto-structural coupling. *J. Phys.: Condens. Matter* **27**, 016005 (2014).
45. Fruchter, L. et al. Electrochemical oxygen intercalation into Sr_2IrO_4. *J. Phys. Chem. Solids* **112**, 1–7 (2018).
46. Sharma, P., Singh, S., Kuga, K., Takeuchi, T. & Bindu, R. Synthesis and structural link to the electronic and magneto-transport properties of spin–orbit Mott insulator Sr_2IrO_4. *J. Phys.: Condens. Matter* **34**, 435402 (2022).